Engineering Structures 61 (2014) 99–112

Contents lists available at ScienceDirect

Engineering Structures

journal homepage: www.elsevier.com/locate/engstruct

Prediction of shear strength of FRP-reinforced concrete flexural members without stirrups using artificial neural networks

S. Lee, C. Lee *

School of Architecture and Building Science, Chung-Ang University, Seoul 156-756, Republic of Korea

ARTICLE INFO

Article history:
Received 8 April 2012
Revised 23 December 2013
Accepted 3 January 2014
Available online 6 February 2014

Keywords:
FRP
Shear
Theoretical modeling
Artificial neural network
Concrete

ABSTRACT

A theoretical model based on an artificial neural network (ANN) was presented for predicting shear strength of slender fiber reinforced polymer (FRP) reinforced concrete flexural members without stirrups. The model takes into account the effects of the effective depth, shear span-to-depth ratio, modulus of elasticity and ratio of the FRP flexural reinforcement and compressive concrete strength on shear strength. Comparisons between the predicted values and 106 test data showed that the developed ANN model resulted in improved statistical parameters with better accuracy than other existing equations. From the 2^k experiment, the influence of parameters was identified in the order of effective depth, axial rigidity of FRP flexural reinforcement, shear span-to-depth ratio and compressive concrete strength. Using the ANN model and based on the results of the 2^k experiment, predictive formulas for shear strength of slender FRP-reinforced concrete beam without stirrups were developed for practical applications. These formulas were able to predict the shear strength better than other existing equations.

1. Introduction

Fiber-reinforced polymers (FRPs) have several advantages over steel, including being non-corrosive and non-magnetic and having higher tensile strength. They are also lighter than steel, which enables easier handling and reduces self-weight of structures. However, they also have the disadvantages of linear elastic tensile behavior that is prone to rupture with lower ductility, lower modulus of elasticity and lower shear strength than steel.

Concrete flexural members that are reinforced with longitudinal steel bars for flexure without stirrups resist the applied shear stresses via a number of mechanisms [1–4], including: (1) shear resistance of uncracked concrete, (2) interlocking action of aggregate, (3) dowel action of the longitudinal reinforcement, (4) arch action, and (5) residual tensile stresses across cracks. Although the basic shear resistance mechanism may be similar to that of steel reinforced concrete members, the distinctive material property of FRPs could significantly alter the relative contribution of each mechanism to the total shear resistance [5–8].

In a beam longitudinally reinforced with less stiff FRP bars, flexural cracks could penetrate deeper into the section and wider cracks will form compared to those in a beam reinforced with an equal amount of longitudinal steel bars with higher stiffness. Deeper flexural cracks with FRP bars would decrease the depth of the compression zone, thereby reducing the contribution of the uncracked concrete to the shear strength [9]. The development of wider and deeper cracks also reduces the resistance by aggregate interlock and the residual tension in cracked concrete. The dowel resistance of longitudinal bars that limit the shearing displacement along the cracks was considered negligible for FRP bars due to their low transverse modulus and smaller size together with relatively wider cracks [1,8].

For the flexural members with a shear span-to-depth ratio a/d of approximately less than 2.5, the arch action occurs [1], in which a and d are the shear span and effective depth of a beam, respectively. Compared to the amount of research on the arch actions for flexural members that are longitudinally reinforced with steel bars, a limited number of studies were reported for the beams with FRP bars [10]. For the slender flexural members with a/d greater than 2.5, the shear strength of flexural members with longitudinal steel bars is a function of a/d as well [11–13]. For these members, a/d represents the interacting effect of the moment (M_f) and shear (V_f) at a section or the quantity $(V_f \cdot d/M_f)^{-1}$ on the shear strength of that section. El-Sayed et al. [14] reported that the experimental shear capacity of the test beams increased as the concrete compressive strength (f_c') increased.

Various design equations have been developed to determine the shear strength of FRP-reinforced concrete flexural members without stirrups [2,6–8,15–21]. Their accuracy, however, seems

* Corresponding author. Tel.: +82 2 820 5872; fax: +82 2 812 4150.
E-mail address: cdlee@cau.ac.kr (C. Lee).

0141-0296/$ - see front matter © 2014 Elsevier Ltd. All rights reserved.
http://dx.doi.org/10.1016/j.engstruct.2014.01.001

limited as these equations were empirically developed using predefined forms and with the test data mainly generated for a limited number of influential parameters.

An artificial neural network (ANN) is a generalized mathematical model of human neural biology. The main feature of an ANN is its ability to classify the data and determine the relationships between the input values (or parameters affecting shear strength) and their outcome (or shear strength). This feature enables an ANN to generalize the effect of each parameter on the shear strength, even if large portions of the data were generated for the purpose of identifying the effects of a limited number of influential parameters. An ANN does not require a predetermined form of equation as in the case of the most empirical approaches. In this study, the development of an ANN model is presented to predict the shear strength of slender FRP-reinforced concrete flexural members without stirrups (V_{cf}).

2. Design equations for shear strength of FRP-reinforced concrete beams without stirrups

2.1. Design equations

The existing equations for V_{cf} are presented in Eqs. (1)–(3), (4a), (4b), (5a), (5b), (6)–(11). Significant gaps exist in selecting the main parameters and their effects on V_{cf} because these equations have been empirically derived. In the following equations, b_w = member web width; d = member effective depth; E_c, E_s and E_f = moduli of elasticity for concrete, steel and FRP, respectively; f_{cu} = cube compressive strength of concrete; $n = E_f/E_c$; β_1 = rectangular compressive stress block parameter for flexure; and ρ_f = flexural FRP reinforcement ratio.

ACI Committee 440 [15]:

$$V_{cf} = \frac{\rho_f \cdot E_f}{90\beta_1 f_c'}\left(\frac{\sqrt{f_c'}b_w d}{6}\right) \tag{1}$$

ACI440.1R-06 [16]:

$$V_{cf} = \frac{2}{5}k_n\sqrt{f_c'}b_w d \tag{2}$$

where $k_n = \sqrt{2\rho_f n + (\rho_f n)^2} - \rho_f n$

BISE design guidelines [17]:

$$V_{cf} = 0.79\left(100\rho_f\frac{E_f}{E_s}\right)^{1/3}\left(\frac{400}{d}\right)^{1/4}\left(\frac{f_{cu}}{25}\right)^{1/3}b_w d \tag{3}$$

CSA S806-02 [18]:

$$\text{For } d \leqslant 300\text{ mm}: \quad V_{cf} = 0.035\lambda\phi_c\left(f_c'\rho_f E_f\frac{V_f}{M_f}d\right)^{1/3}b_w d$$
$$0.1\lambda\phi_c\sqrt{f_c'}b_w d \leqslant V_{cf} \leqslant 0.2\lambda\phi_c\sqrt{f_c'}b_w d \tag{4a}$$

$$\text{For } d > 300\text{ mm}: \quad V_{cf} = \left(\frac{130}{1000+d}\right)\lambda\phi_c\sqrt{f_c'}b_w d$$
$$\geqslant 0.08\lambda\phi_c\sqrt{f_c'}b_w d\frac{V_f}{M_f}d \leqslant 1.0 \quad (\lambda = 1.0 \text{ and } \phi_c = 1.0 \text{ for the present study}) \tag{4b}$$

ISIS-M03-01 [19]:

$$\text{For } d \leqslant 300\text{ mm}: V_{cf} = 0.2\lambda\phi_c \cdot \sqrt{f_c'}b_w d\sqrt{\frac{E_f}{E_s}} \tag{5a}$$

$$\text{For } d > 300\text{ mm}: \quad V_{cf} = \left[\frac{260}{1,000+d}\right]\lambda\phi_c \cdot \sqrt{f_c'}b_w d\sqrt{\frac{E_f}{E_s}}$$
$$\geqslant 0.1\lambda\phi_c\sqrt{f_c'} \cdot b_w d\sqrt{\frac{E_f}{E_s}} \tag{5b}$$

JSCE shear design method [20]:

$$V_{cf} = \beta_d\beta_\rho\beta_n f_{vcd}b_w d/\gamma_b \tag{6}$$

where

$$V_{cf} = \beta_d\beta_\rho\beta_n f_{vcd}b_w d/\gamma_b$$

$$f_{vcd} = 0.2(f_c')^{(1/3)} \leqslant 0.72$$

$$\beta_d = \left(\frac{1000}{d}\right)^{(1/4)} \leqslant 1.5$$

$$\beta_\rho = \left(100\rho_f\frac{E_f}{E_s}\right)^{(1/3)} \leqslant 1.5$$

$$\beta_n = \begin{cases} 1 + \frac{M_o}{M_d} \leqslant 2 \text{ for the } N_d' \geqslant 0 \\ 1 + \frac{M_o}{M_d} \geqslant 0 \text{ for the } N_d' < 0 \end{cases}$$

γ_b = 1.0 for the present day.

Michaluk et al. [7]:

$$V_{cf} = \frac{E_f}{E_s}\left(\frac{1}{6}\sqrt{f_c'}b_w d\right) \tag{7}$$

Deitz et al. [6]:

$$V_{cf} = 3\frac{E_f}{E_s}\left(\frac{1}{6}\sqrt{f_c'}b_w d\right) \tag{8}$$

Tureyen and Frosch [21]:

$$V_{cf} = \frac{5}{12}k_n\sqrt{f_c'}b_w d \tag{9}$$

El-Sayed et al. [2]:

$$V_{cf} = \left(\frac{\rho_f E_f}{90\beta_1 f_c'}\right)^{1/3}\left(\frac{\sqrt{f_c'}}{6}b_w d\right) \leqslant \frac{\sqrt{f_c'}}{6}b_w d \tag{10}$$

Razaqpur and Isgor [8]:

$$V_{cf} = 0.035k_m k_s k_a(1+k_r)\sqrt{f_c'}b_w d \leqslant 0.2k_s\sqrt{f_c'}b_w d \tag{11}$$

where

$$k_m = \left(\frac{V_F d}{M_F}\right)^{2/3}$$

$$k_r = (E_f\rho_f)^{1/3}$$

$$k_a = \begin{cases} 1.0 & \text{for } \left(\frac{M_f}{V_f d}\right) \geqslant 2.5 \\ \frac{2.5}{(M_f/V_f d)} & \text{for } \left(\frac{M_f}{V_f d}\right) < 2.5 \end{cases}$$

$$k_s = \begin{cases} 1.0 & \text{for } d \leqslant 300\text{ mm} \\ \frac{750}{450+d} & \text{for } d > 300\text{ mm} \end{cases}$$

2.2. Limitations of the existing equations

Table 1 summarizes the parameters included in Eqs. (1)–(3), (4a), (4b), (5a), (5b), (6)–(11). The error metrics in terms of the

Table 1
Experimental to predicted shear strengths for beams without stirrups.

Equations or models	Eqs.	Design parameters							Statistical parameters on $V^p_{cf,s}/V^t_{cf,s}$				
		f'_c	b_w	d	E_f	ρ_f	$E_f\rho_f$	a/d	μ	σ	COV	RMSE	R^2
ACI Committee 440 [15]	(1)	O	O	O	–	–	O	–	3.74	1.47	0.39	0.44	0.78
ACI440.1R-06 [16]	(2)	O	O	O	–	–	O	–	1.80	0.38	0.21	0.35	0.95
BISE [17]	(3)	O	O	O	–	–	O	–	1.08	0.25	0.23	0.21	0.92
CSA S806-02 [18]	(4)	O	O	O	–	–	O	O	1.29	0.38	0.30	0.28	0.81
ISIS-M03-01 [19]	(5)	O	O	O	O	–	–	–	1.27	0.38	0.30	0.29	0.82
JSCE [20]	(6)	O	O	O	–	–	O	–	1.29	0.28	0.21	0.27	0.93
Michaluk et al. [7]	(7)	O	O	O	O	–	–	–	3.00	1.29	0.43	0.42	0.58
Deitz et al. [6]	(8)	O	O	O	O	–	–	–	1.00	0.43	0.43	0.35	0.58
Tureyen and Frosch [21]	(9)	O	O	O	–	–	O	–	1.73	0.37	0.21	0.35	0.95
El-Sayed et al. [2]	(10)	O	O	O	–	–	O	–	1.30	0.23	0.18	0.27	0.95
Razaqpur and Isgor [8]	(11)	O	O	O	–	–	O	O	0.90	0.19	0.21	0.23	0.90
AV641.41	model	O	O	O	O	O	–	O	1.01 (1.02)	0.14 (0.15)	0.14 (0.15)	0.16 (0.16)	0.98 (0.97)
AV_{bd}541.41	model	O	O	O	O	O	–	O	1.04 (1.05)	0.14 (0.12)	0.13 (0.11)	0.18 (0.19)	0.95 (0.94)
AV_b441.41	model	O	O	O	–	–	O	O	1.03 (1.04)	0.15 (0.14)	0.15 (0.14)	0.18 (0.19)	0.95 (0.94)
Proposed Eq.	(19)	O	O	O	O	O	O	O	1.01	0.16	0.16	0.19	0.94
	(20)	O	O	O	O	O	O	O	1.00	0.19	0.19	0.18	0.96

$\mu = \frac{\sum_{i=1}^{n_d} V^t_{cf,i}/V^p_{cf,i}}{n_d}$, $\sigma = \sqrt{\frac{\sum_{i=1}^{n_d}\left(V^t_{cf,i}/V^p_{cf,i}-\mu\right)^2}{n_d}}$, $RMSE = \sqrt{\frac{\sum_{i=1}^{n_d}\left(V^{p,s}_{cf,i}-V^{t,s}_{cf,i}\right)^2}{n_d}}$, $R^2 = \frac{n_d \cdot S_{tp} - S_t \cdot S_p}{\sqrt{n_d \cdot S_{tt} - S_t^2}\cdot\sqrt{n_d \cdot S_{pp} - S_p^2}}$ in which $S_{tp} = \sum_{i=1}^{n_d}(V^t_{cf,i}\cdot V^p_{cf,i})$; $S_t = \sum_{i=1}^{n_d} V^t_{cf,i}$; $S_p = \sum_{i=1}^{n_d} V^p_{cf,i}$; $S_{tt} = \sum_{i=1}^{n_d}(V^t_{cf,i})^2$; and $S_{pp} = \sum_{i=1}^{n_d}(V^p_{cf,i})^2$.

average (μ), standard deviation (σ), coefficient of variation (COV), root mean square error (RMSE) and squared correlation coefficient (R^2) between the standardized ith predicted and target values of V_{cf} ($V^{p,s}_{cf,i}$ and $V^{t,s}_{cf,i}$) are also presented in Table 1. The inconsistencies of the existing equations for predicting V_{cf} have been pointed out by different researchers [8,22,23]. Review on their criticisms and some additional comments made by the authors are summarized as follows: an insufficient number of necessary parameters as can be seen in Table 1 (Eqs. (1)–(3), (5–10)); contradictions to experimental evidence such as V_{cf} being inversely proportional to $\sqrt{f'_c}$ (Eq. (1)); no lower or upper limits on V_{cf} (Eqs. (1)–(3), and (7)–(11)); improper inclusion of the linear elastic properties of concrete for shear failure at the ultimate state (parameter k_n in Eqs. (2) and (9)); inaccurate predictions for a particular parameter in its certain range – underestimation for a/d less than 2.5 and overestimation for the beam with $d \geqslant 300$ mm in Eq. (4)); the main mechanisms directly adopted from the test results of concrete flexural members reinforced with longitudinal steel bars (arch action adopted from Zutty's equation [11] and the effect of moment at a section on its shear resistance from [13]), insufficient number of test data to verify the size effect in Eq. (11) and accuracy estimation based on insufficient data (verification of Eq. (11) with 63 data, for example).

Inconsistent expressions of predictive equations might have been also attributed to the data mostly generated in relation to the effect of axial rigidity of FRP bars ($E_f \cdot \rho_f$) and a relative lack of experimental results on the effects of the other parameters. For example, the portions of concrete strength contributing to V_{cf} were given by $(f'_c)^p$ with the exponent p in the range of $-1/2 \leqslant p \leqslant 1/2$; effective depth by $(d)^p$ with For $p = 1$ multiplied by a factor of size effect, $d/(N + d)$ in Eqs. (4), (5), and (11) for $d \geqslant 300$ mm, where N is an equation-specific number, or $3/4 \leqslant p \leqslant 1$ in other equations; shear span-to-depth ratio by $(a/d)^p$ with $p = -5/3$ for $a/d < 2.5$ and $p = -2/3$ for $a/d \geqslant 2.5$ in Eq. (11) or $p = -1/3$ in Eq. (4) for $d \geqslant 300$ mm; flexural reinforcement ratio of FRP by $(\rho_f)^p$ with $p = 0$ in Eqs. (5), (7) and (8); modulus of elasticity of FRP by $(E_f)^p$ with $1/2 \leqslant p \leqslant 1$ in Eqs. (5), (7) and (8); and axial rigidity of flexural FRP reinforcement by $(E_f \cdot \rho_f)^p$ with $1/3 \leqslant p \leqslant 1.0$ in Eqs. (1–4), (6) and (9)–(11).

To take full advantage of the positive material properties of FRPs in addition to their non-corrosiveness, a more reliable model for predicting V_{cf} is needed. Since the ANN is able to classify the data and generalize the relationships between parameter sets and the corresponding shear strength, the aforementioned limitations found in the equations derived from the conventional empirical approach can be overcome resulting in more accurate V_{cf} predictions.

3. Development of ANN model

3.1. Network architecture

The ANN is developed with the assumption that information processing occurs at elements called neurons. Signals are passed between neurons over the weighted connection links, and each neuron applies an activation function to its net input to determine its output signal [24]. Fig. 1 schematically shows the architecture of a four-layer neural network based on back-propagation: one input layer, two hidden layers and one output layer. The number of input neurons depends on the selection of the main parameters that would influence V_{cf}. The output layer consists of one neuron for which the experimentally observed V_{cf} values are assigned as target values for the given set of input parameters.

To avoid a slow rate of learning near the end points of the output range, the standardization function was used, which converts values of each input parameter and experimentally measured shear strength into bipolar numbers:

$$s_{I,i} = (s_{I,\max} - s_{I,\min}) \cdot \frac{(v_{I,i} - v_{I,\min})}{(v_{I,\max} - v_{I,\min})} + s_{I,\min} \qquad (12)$$

where $s_{I,i}$ is the standardized number of the Ith input parameter for the ith set of parameters in the data (or shear strength); $s_{I,\max}$ and $s_{I,\min}$ are maximum and minimum values of $s_{I,i}$ for $1 \leqslant i \leqslant 106$ parameter sets in the data (=0.95 and 0.05, respectively in this study); and $v_{I,i}$, $v_{I,\min}$ and $v_{I,\max}$ are values of the Ith input parameter in the ith set of parameters in the data (or measured shear strength) and their corresponding minimum and maximum values in the data, respectively.

The error function (E) is defined in Eq. (13) which measures the difference between the standardized predicted shear strengths ($V^{p,s}_{cf,i}$) obtained by the standardized input parameters ($s_{I,i}$) and the

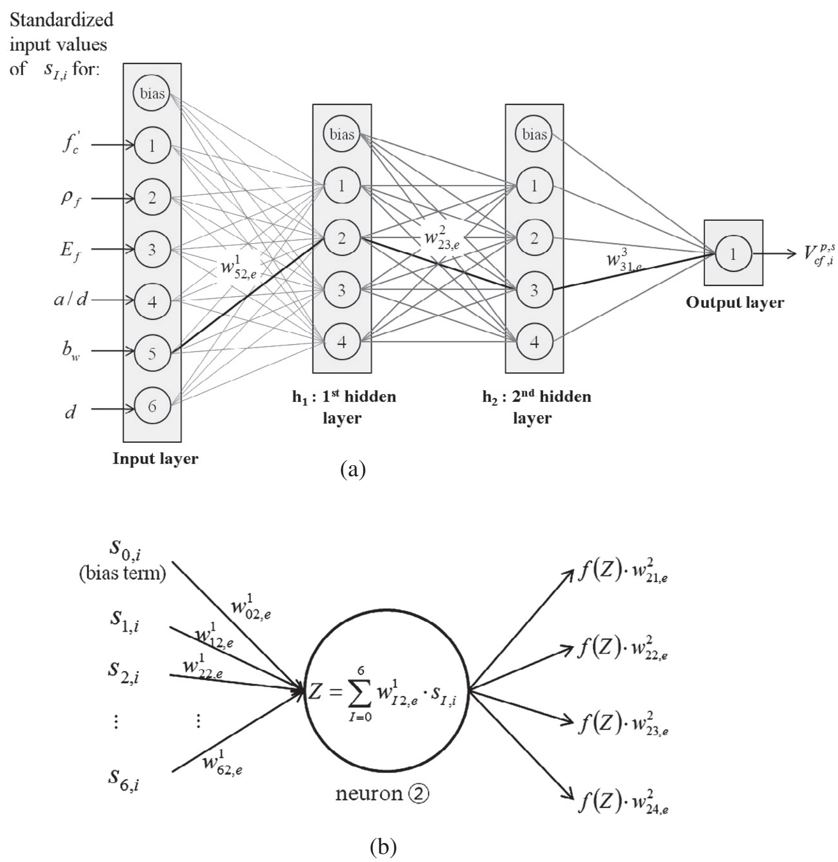

Fig. 1. The architecture of *AV*641.41 model at the *e*th epoch. (a) Architecture (b) Neuron ② in the first hidden layer, h_1 (c) ($s_{I,i}$ = standardized value of the *I*th parameter for the *i*th set in the data (Eq. (12)).

target shear strengths ($V^{t,s}_{cf,i}$) obtained from test results and standardized by the rule of Eq. (12):

$$E = \frac{1}{2}\sum_{i=1}^{n_d}(V^{p,s}_{cf,i} - V^{t,s}_{cf,i})^2 \tag{13}$$

where n_d = number of parameter sets in the data = 106 in this study.

The error function in Eq. (13) is the function of weights. These weights are iteratively updated based on the gradient descent method until the pre-assigned tolerance is satisfied or the number of iteration reaches the pre-assigned maximum number of iterations. In this study, the tolerance of 0.1 is given for RMSE between the standardized *i*th predicted and target values of $V_f(V^{p,s}_{cf,i}$ *and* $V^{t,s}_{cf,i})$. The sigmoid function, $f(Z)=1/(1+\exp(-Z))$, is used as an activation function, where Z is the multiplication of the steepness parameter by the weighted sum of the inputs from the preceding layers. Using the sigmoidal activation function, a large number of hidden neurons could either lead to a solution surface that deviates considerably from the trend of the surface at the intermediate points or provide a too literal interpretation of the training points [25,26]. Proper determination of the number of neurons in a hidden layer is to some extent problem-specific in predicting the target values with reasonable accuracy without disturbing the stability of the network [27]. Different researchers have adopted different number of hidden layers in predicting structural performance: one hidden layer by Oreta [28], Mansour et al. [27], and Cladera and Mari [29]; and two hidden layers by Jung and Kim [30]. In this study, architectures with either one or two hidden layers were tested. Momentum is added to the weight update formulas as given in Eq. (14) to improve the convergence rate:

$$\Delta w^l_{jk,e+1} = \alpha \cdot \delta_k \cdot z_j + \theta \cdot \Delta w^l_{jk,e} \tag{14}$$

where $\Delta w^l_{jk,e+1}$ is the modification of the weight of the connection link between the *j*th node in the *l*th layer and the *k*th node in $(l+1)$th layer for weights at the $(e+1)$th epoch=$\Delta w^l_{jk,e} - \Delta w^l_{jk,e-1}$; $\Delta w^l_{jk,e}$ the weight of the connection link between the *j*th node in the *l*th layer and the *k*th node in the $(l+1)$th layer at the *e*th epoch; α *and* θ the learning rate and the momentum parameter, respectively; δ_k the portion of error correction weight adjustment for $\Delta w^l_{jk,e+1}$; and z_j is the input to the *k*th node of the $(l+1)$th layer from the *j*th node of the *l*th layer.

In Eq. (14), the momentum parameter θ is constrained to be in the range from 0.0 to 1.0, exclusive of the end points [24].

3.2. Selection of input parameters and target value

Research has shown that V_{cf} is mainly dependent on six parameters: compressive concrete strength (f_c'), flexural reinforcement ratio (ρ_f), modulus of elasticity of FRP bar (E_f), shear span depth ratio (a/d), width of web (b_w) and effective depth (d) [2,5–9]. The input layer could primarily consist of six input neurons assigned for these six parameters. In this case, the target values could be either shear strength (V_{cf}) or shear stress ($V_{cf}/(b_w d)$).

It is generally agreed that the shear strength of reinforced concrete flexural members is linearly proportional to the member width (b_w). This allows for the exclusion of the member width from the set of input parameters and the ANN to be trained for the target values of the normalized shear strength with respect to the member width (V_{cf}/b_w) or shear stress ($V_{cf}/(b_w d)$).

The axial rigidity of FRP longitudinal reinforcement ($E_f\ \rho_f$) is known to be a controlling influential parameter that determines the V_{cf} Experimental findings have also suggested that the shear strength is linearly proportional to either $E_f \cdot \rho_f$ (Eq. (1)) or $(E_f \cdot \rho_f)^{1/3}$

(Eqs. (3) and (9)). This implies that input by $E_f \cdot \rho_f$ would better reflect the physical shear resistance mechanism than would separate inputs by individual ρ_f and E_f. The target values in the output neuron could be either shear strength (V_{cf}) or shear stress ($V_{cf}/(b_w d)$) in this case.

Accordingly, six types of architecture were considered in this study (Table 2). The ANN architecture is labeled as $AV_t n_i n_{h1} n_{h2} n_o \cdot v_\alpha v_\theta$. The subscript '$t$' in AV represents the type of target values (AV, AV_b and AV_{bd} for the target values of V_{cf}, V_{cf}/b_w and $V_{cf}/b_w d$, respectively); n_i for the number of neurons in input layer (4, 5 or 6); n_{h1} and n_{h2} for the number of neurons in the first and the second hidden layers; n_o for the number of neurons in the output layer (=1); v_α for parameter value of the learning rate (v_α = 1, 2, 3 and 4 for α = 0.1, 0.2, 0.3 and 0.4, respectively); and v_θ = 1 and 2 for μ = 0.1 and 0.2, respectively.

3.3. Experimental data

Table 3 lists 110 data points that were considered in this research. The data were collected from 18 different test results on V_{cf} for beams and slabs [2,4,6,7,9,14,23,31–41]. Some data in Table 3, however, were excluded from the analysis: beam no.28 and beam no.101 were reported to have failed prematurely due to the loss of anchorage; beam no. 29 with a/d = 1.82 (<2.5) was under the influence of arch action [11]; and beam no. 32 had a value of d = 970 mm. As there were no intermediate data bridging the large gap in effective depth between d = 360 mm and 970 mm, beam no. 32 was excluded to avoid misleading classification of the size effect by the ANN.

The 110 data were ultimately reduced to 106 data and randomly grouped into two subsets: a training set of 77 data and a testing set of 29 data – approximately 73% and 27% of the 106 data, respectively. The training set is used to compute the gradient and update the network weights and biases to minimize the training error. When the error on the testing set that is monitored during the training process increases for a specified number of iterations, the training is stopped and the network weights and biases at the minimum testing error are returned [42]. Table 4 shows the similarities that exist in the statistical parameters among the total, training, and testing data with respect to μ, σ, coefficient of variation (COV), and the minimum and maximum values.

3.4. Training of the ANN model

The ANN performance significantly depends on the initial conditions, initial weights, biases, back-propagation algorithms, and learning rate [43]. In this research, various values for each parameter were tested to determine the best-performing ANN model: the number of hidden layers with 1 or 2, the number of hidden nodes with 4, 6 or 8, the values of learning rate (α) in the range of 0.1–0.4 in intervals of 0.1 and the momentum parameter (θ) with 0.1 or 0.2. Upon the performance observation of the developed ANN model, the maximum number of epochs was empirically set to 3000 and the performance of the candidate ANN model was estimated by the RMSE. It was observed that although the RMSE with respect to the training data tended to decrease monotonically, the RMSE resulting from the testing data tended to decrease and then increase as the epoch increased.

In this study, if the sum of the RMSEs from both the training and the testing data at the current epoch becomes less than the sum of RMSEs from the previous epoch, then the weights between the nodes in each layer at the current epoch were saved. During the elapse of the maximum 3000 epochs, the weights that resulted in the minimum sum on RMSEs were assigned to the given architecture, which could be considered the best predictor for the given set of parameters.

After training 288 different networks, the ANN models with the best results based on the lowest RMSE among the different sets of parameters for the given architecture were chosen and are tabulated in Table 2. The error metrics in terms of the average (μ), standard deviation (σ), coefficient of variation (COV), RMSE and squared correlation coefficient (R^2) are given in Table 2. The best ANN models selected from a set of the same number of input parameters include: the AV_b441.41 with four inputs; the AV_{bd}541.41 with five inputs; and the AV641.41 with six inputs. Their error metrics were given with bold values in Table 2. Among these, the AV641.41 model has shown the most improved values of statistical parameters: the average, standard deviation, COV, RMSE and R^2 of the AV641.41 model were 1.01, 0.14, 0.14, 0.16 and 0.98, respectively, for the total data, 1.00, 0.14, 0.14, 0.15 and 0.98, respectively, for the training data, and 1.02, 0.15, 0.15, 0.16 and 0.97, respectively, for testing data.

For accuracy validation, the predictions by the AV641.41 model were compared to the existing equations. Parametric studies were also conducted with the AV641.41 model to further verify its ability to simulate the effects of influential parameters on V_{cf}.

4. Validity of the developed *AV*641.41 model

4.1. Comparisons with the existing predictive equations

In Table 1, the statistical parameters are presented for the ratios of the predicted shear strengths to the experimentally measured shear strengths for 106 data. The values of the statistical parameters presented in Table 1 indicate that the developed AV641.41 model predicts the experimental results better than other design codes or equations.

Table 2
ANN architectures and values of their statistical parameters on $V^p_{cf,s}/V^t_{cf,s}$.

Models	No. of input nodes	Input parameters	Output parameters	Statistical parameters				
				μ	σ	COV	RMSE	R^2
AV_b441.41	4	$f_c', E_f \cdot \rho_f, a/d, d$	V_{cf}/b_w	**1.03 (1.04)**	**0.15 (0.14)**	**0.15 (0.14)**	**0.18 (0.19)**	**0.95 (0.94)**
AV_b4881.42				1.04	0.15	0.14	0.19	0.94
AV_{bd}441.42			$V_{cf}/b_w d$	1.04	0.15	0.14	0.19	0.94
AV_{bd}4661.11				1.02	0.15	0.15	0.19	0.93
AV_b581.42	5	$f_c', E_f, \rho_f a/d, d$	V_{cf}/b_w	1.04	0.15	0.14	0.19	0.94
AV_b5441.31				1.03	0.15	0.15	0.19	0.93
AV_{bd}541.41			$V_{cf}/b_w d$	**1.04 (1.05)**	**0.14 (0.12)**	**0.13 (0.11)**	**0.18 (0.19)**	**0.95 (0.94)**
AV_{bd}5441.41				1.05	0.15	0.14	0.19	0.94
AV641.41	6	$f_c', E_f, \rho_f a/d, b_w, d$	V_{cf}	**1.01 (1.02)**	**0.14 (0.15)**	**0.14 (0.14)**	**0.16 (0.16)**	**0.98 (0.97)**
AV6441.41				1.04	0.16	0.15	0.17	0.97
AV_{bd}681.31			$V_{cf}/b_w d$	1.03	0.14	0.14	0.18	0.95
AV_{bd}6661.41				1.04	0.13	0.13	0.17	0.96

Note: Values in parentheses present value of error metrics for testing data only.

Table 3
Data list.

No	f'_c (MPa)	$\rho_f(\times 10^{-2})$	E_f (MPa)	$E_f \cdot \rho_f$ (MPa)	a/d	b_w (mm)	d (mm)	V_{cf} (N)	Ref.	Comment
1	40.0	0.39	114,000	440	6.05	1000	165.3	140,000	[31]	
2	40.0	0.78	114,000	890	6.05	1000	165.3	167,000	[31]	
3	40.0	1.18	114,000	1350	6.23	1000	160.5	190,000	[31]	
4	40.0	0.86	40,000	340	6.17	1000	162.1	113,000	[31]	
5	40.0	1.70	40,000	680	6.29	1000	159.0	142,000	[31]	
6	40.0	1.71	40,000	680	6.17	1000	162.1	163,000	[31]	
7	40.0	2.44	40,000	980	6.29	1000	159.0	163,000	[31]	
8	40.0	2.63	40,000	1050	6.49	1000	154.1	168,000	[31]	
9	50.0	0.87	128,000	1110	3.07	250	326.0	77,500	[2]	
10	50.0	0.87	39,000	340	3.07	250	326.0	70,500	[2]	
11	44.6	1.24	134,000	1660	3.07	250	326.0	104,000	[2]	
12	44.6	1.22	42,000	510	3.07	250	326.0	60,000	[2]	
13	43.6	1.72	134,000	2300	3.07	250	326.0	124,500	[2]	
14	43.6	1.71	42,000	720	3.07	250	326.0	77,500	[2]	
15	63.0	1.71	135,000	2310	3.07	250	326.0	130,000	[14]	
16	63.0	1.71	42,000	720	3.07	250	326.0	87,000	[14]	
17	63.0	2.20	135,000	2970	3.07	250	326.0	174,000	[14]	
18	63.0	2.20	42,000	920	3.07	250	326.0	115,500	[14]	
19	28.9	0.45	38,000	170	3.98	150	167.5	12,500	[32]	
20	28.9	0.71	32,000	230	3.14	150	212.3	17,500	[32]	
21	28.9	0.86	32,000	280	2.53	150	263.0	25,000	[32]	
22	50.2	1.39	32,000	440	4.10	150	162.6	17,500	[32]	
23	50.2	1.06	32,000	340	3.13	150	213.3	27,500	[32]	
24	50.2	1.15	32,000	370	2.54	150	262.1	30,000	[32]	
25	40.5	0.25	145,000	360	2.67	200	225.0	36,100	[33]	
26	49.0	0.50	145,000	730	2.67	200	225.0	47,000	[33]	
27	40.5	0.63	145,000	910	2.67	200	225.0	47,200	[33]	
28	40.5	0.88	145,000	1280	2.67	200	225.0	42,700	[33]	Excluded
29	40.5	0.50	145,000	730	1.82	200	225	96,180	[33]	Excluded
30	40.5	0.50	145,000	730	3.78	200	225.0	49,700	[33]	
31	40.5	0.50	145,000	730	4.22	200	225.0	38,500	[33]	
32	40.0	0.46	40,000	180	3.14	450	970	136,000	[34]	Excluded
33	60.3	0.33	139,000	460	6.36	127	143.0	14,300	[35]	
34	60.3	0.33	139,000	460	6.36	127	143.0	12,900	[35]	
35	60.3	0.33	139,000	460	6.36	127	143.0	14,700	[35]	
36	61.8	0.58	139,000	810	6.45	159	141.0	19,800	[35]	
37	61.8	0.58	139,000	810	6.45	159	141.0	23,100	[35]	
38	61.8	0.58	139,000	810	6.45	159	141.0	17,000	[35]	
39	81.4	0.47	139,000	650	6.36	89	143.0	8800	[35]	
40	81.4	0.47	139,000	650	6.36	89	143.0	11,700	[35]	
41	81.4	0.47	139,000	650	6.36	89	143.0	8900	[35]	
42	81.4	0.76	139,000	1060	6.45	121	141.0	14,300	[35]	
43	81.4	0.76	139,000	1060	6.45	121	141.0	15,300	[35]	
44	81.4	0.76	139,000	1060	6.45	121	141.0	16,600	[35]	
45	37.3	0.72	42,000	300	2.75	160	346.0	54,500	[36]	
46	37.3	0.72	42,000	300	2.75	160	346.0	63,700	[36]	
47	43.2	1.10	42,000	460	3.32	160	346.0	42,700	[36]	
48	43.2	1.10	42,000	460	3.32	160	346.0	42,500	[36]	
49	34.1	1.54	42,000	650	3.54	160	325.0	48,700	[36]	
50	34.1	1.54	42,000	650	3.54	160	325.0	44,900	[36]	
51	37.3	0.72	120,000	860	3.06	130	310.0	49,200	[36]	
52	37.3	0.72	120,000	860	3.06	130	310.0	45,800	[36]	
53	43.2	1.10	120,000	1320	3.71	130	310.0	47,600	[36]	
54	43.2	1.10	120,000	1320	3.71	130	310.0	52,700	[36]	
55	34.1	1.54	120,000	1850	3.71	130	310.0	55,900	[36]	
56	34.1	1.54	120,000	1850	3.71	130	310.0	58,300	[36]	
57	79.6	1.25	40,300	500	4.06	203	225.0	41,600	[23]	
58	79.6	1.25	40,300	500	4.06	203	225.0	30,400	[23]	
59	79.6	1.25	40,300	500	4.06	203	225.0	42,100	[23]	
60	79.6	1.66	40,300	670	4.06	152	225.0	31,000	[23]	
61	79.6	1.66	40,300	670	4.06	152	225.0	33,100	[23]	
62	79.6	1.66	40,300	670	4.06	152	225.0	33,500	[23]	
63	79.6	2.10	40,300	850	4.08	165	224.0	38,400	[23]	
64	79.6	2.10	40,300	850	4.08	165	224.0	32,200	[23]	
65	79.6	2.10	40,300	850	4.08	165	224.0	36,700	[23]	
66	79.6	2.56	40,300	1030	4.08	203	224.0	48,300	[23]	
67	79.6	2.56	40,300	1030	4.08	203	224.0	45,700	[23]	
68	79.6	2.56	40,300	1030	4.08	203	224.0	45,200	[23]	
69	39.7	0.96	40,500	390	3.39	457	360.0	108,100	[9]	
70	39.9	0.96	37,600	360	3.39	457	360.0	94,700	[9]	
71	40.3	0.96	47,100	450	3.39	457	360.0	114,800	[9]	
72	42.3	1.92	40,500	780	3.39	457	360.0	137,000	[9]	
73	42.5	1.92	37,600	720	3.39	457	360.0	152,600	[9]	
74	42.6	1.92	47,100	900	3.39	457	360.0	177,000	[9]	

Table 3 (*continued*)

No	f'_c (MPa)	$\rho_f (\times 10^{-2})$	E_f (MPa)	$E_f \cdot \rho_f$ (MPa)	a/d	b_w (mm)	d (mm)	V_{cf} (N)	Ref.	Comment
75	36.3	1.11	40,300	450	4.06	229	225.0	39,100	[4]	
76	36.3	1.11	40,300	450	4.06	229	225.0	38,500	[4]	
77	36.3	1.11	40,300	450	4.06	229	225.0	36,800	[4]	
78	36.3	1.42	40,300	570	4.06	178	225.0	28,100	[4]	
79	36.3	1.42	40,300	570	4.06	178	225.0	35,000	[4]	
80	36.3	1.42	40,300	570	4.06	178	225.0	32,100	[4]	
81	36.3	1.66	40,300	670	4.06	229	225.0	40,000	[4]	
82	36.3	1.66	40,300	670	4.06	229	225.0	48,600	[4]	
83	36.3	1.66	40,300	670	4.06	229	225.0	44,700	[4]	
84	36.3	1.81	40,300	730	4.06	279	225.0	43,800	[4]	
85	36.3	1.81	40,300	730	4.06	279	225.0	45,900	[4]	
86	36.3	1.81	40,300	730	4.06	279	225.0	46,100	[4]	
87	36.3	2.05	40,300	830	4.08	254	224.0	37,700	[4]	
88	36.3	2.05	40,300	830	4.08	254	224.0	51,000	[4]	
89	36.3	2.05	40,300	830	4.08	254	224.0	46,600	[4]	
90	36.3	2.27	40,300	910	4.08	229	224.0	43,500	[4]	
91	36.3	2.27	40,300	910	4.08	229	224.0	41,800	[4]	
92	36.3	2.27	40,300	910	4.08	229	224.0	41,300	[4]	
93	24.1	2.30	40,000	920	2.69	178	279.0	53,400	[37]	
94	24.1	0.77	40,000	310	2.61	178	287.0	36,100	[37]	
95	24.1	1.34	40,000	540	2.61	178	287.0	40,100	[37]	
96	28.6	0.73	40,000	290	4.51	305	157.5	26,800	[6]	
97	30.1	0.73	40,000	290	5.80	305	157.5	28,300	[6]	
98	27.0	0.73	40,000	290	5.80	305	157.5	29,200	[6]	
99	28.2	0.73	40,000	290	5.81	305	157.5	28,500	[6]	
100	30.8	0.73	40,000	290	5.82	305	157.5	27,600	[6]	
101	66.0	0.96	41,300	400	12.50	1000	104.0	37,300	[7]	Excluded
102	66.0	0.76	41,300	310	8.44	1000	154.0	79,100	[7]	
103	34.7	1.30	130,00	1690	2.69	200	260.0	62,200	[38]	
104	38.1	1.31	45,000	590	3.65	150	210.0	26,500	[39]	
105	32.9	1.36	45,000	610	3.65	150	210.0	22,000	[39]	
106	38.0	0.36	41,400	150	4.10	305	192.0	26,700	[40]	
107	39.0	1.55	34,000	530	3.15	154	222.0	19,500	[40]	
108	34.3	1.51	105,000	1590	3.00	150	250.0	45,000	[41]	
109	34.3	3.02	105,000	3170	3.00	150	250.0	46,000	[41]	
110	34.3	2.27	105,000	2380	3.00	150	250.0	40,500	[41]	

Table 4
Statistics of experimental data.

		f'_c (MPa)	$\rho_f (\times 10^{-2})$	E_f (MPa)	$E_f \rho_f$ (MPa)	a/d	b_w (mm)	d (mm)	V_{cf} (N)
Total data	No. of data	106	106	106	106	106	106	106	106
	μ	47.49	1.31	70,187	792	4.20	275.48	236.68	57,560
	σ	17.37	0.65	43,780	536.9	1.30	235.79	68.16	43,910
	COV	0.37	0.49	0.62	0.68	0.31	0.86	0.29	0.77
	Min. value	24.1	0.25	32,000	150	2.53	89	141	8800
	Max. value	81.4	3.02	145,000	3170	8.44	1000	360	190,000
Training data	No. of data	77	77	77	77	77	77	77	77
	μ	47.21	1.34	70,340	788	4.23	279.42	237.29	57,003
	σ	16.98	0.65	43,400	483	1.33	245.03	68.56	44,704
	COV	0.36	0.49	0.62	0.61	0.32	0.88	0.29	0.78
	Min. value	24.1	0.25	32,000	171	2.53	89	141	8800
	Max. value	81.4	3.02	145,000	3171	8.44	1000	360	190,000
Testing data	No. of data	29	29	29	29	29	29	29	29
	μ	48.25	1.23	68,731	822	4.13	265.03	235.68	56,208
	σ	18.64	0.63	44,100	676	1.23	212.99	68.15	42,230
	COV	0.39	0.51	0.64	0.82	0.30	0.80	0.29	0.75
	Min. value	28.2	0.36	32,000	150	2.69	89	141	8900
	Max. value	81.4	2.56	145,000	2970	6.45	1000	346	174,000

The statistical parameter values in Table 1 indicates that Eqs. (1), (2), (4–7), (9) and (10) underestimate the experimentally measured shear strengths with the μ and α on $V^t_{cf,i}/V^p_{cf}$ in $1.29 \leqslant \mu \leqslant 3.74$ and $0.37 \leqslant \alpha \leqslant 1.47$. Except for Eq. (4) in these equations, the other equations did not consider the effect of a/d on V_{cf}. Eqs. (4) and (5) exhibited similar trends in their predictions in terms of their statistical parameter values. Eq. (4) did not consider the effect of the FRP axial rigidity for d values greater than 300 mm, whereas Eq. (5) omitted the effect of the FRP reinforcement ratio in its equation. Because most of the experiments described in Table 3 were performed to investigate the FRP axial rigidity, the equations that did not account for the FRP axial rigidity (Eq. (4)) or the FRP reinforcement ratio (Eqs. (5), (7) and (8)) showed more scattering. Among these equations, Eqs. (6) and (10) showed relatively improved statistical values compared to the other equations (Table 1).

Although Eq. (8) resulted in the average of 1.0 on $V^t_{cf,i}/V^p_{cf,i}$, its accuracy was greatly hindered by large α, COV and RMSE and by low R^2 values. The values of statistical parameters for the remaining equations (Eqs. (3) and (11)) indicate that these equations predicted the experimental results better than other existing equations.

Based on the aforementioned discussion, Eqs. (3), (6), (10), and (11) and the developed *AV*641.41 model, which showed better statistical parameter values than the other ANN models, are considered in a further investigation of the effect of the parameters on V_{cf}. They have statistical parameter values in the range of $0.9 \leqslant \mu \leqslant 1.30$, $0.14 \leqslant \alpha \leqslant 0.28$, $0.14 \leqslant COV \leqslant 0.23$, $0.16 \leqslant RMSE \leqslant 0.27$ and $0.90 \leqslant R^2 \leqslant 0.98$. Comparisons between the test results and their predictions on V_{cf} are presented in Fig. 2. The predictions on V_{cf} made by the developed *AV*641.41 model showed better correlation to the experimentally observed ones than those by Eqs. (3), (6), (10), and (11).

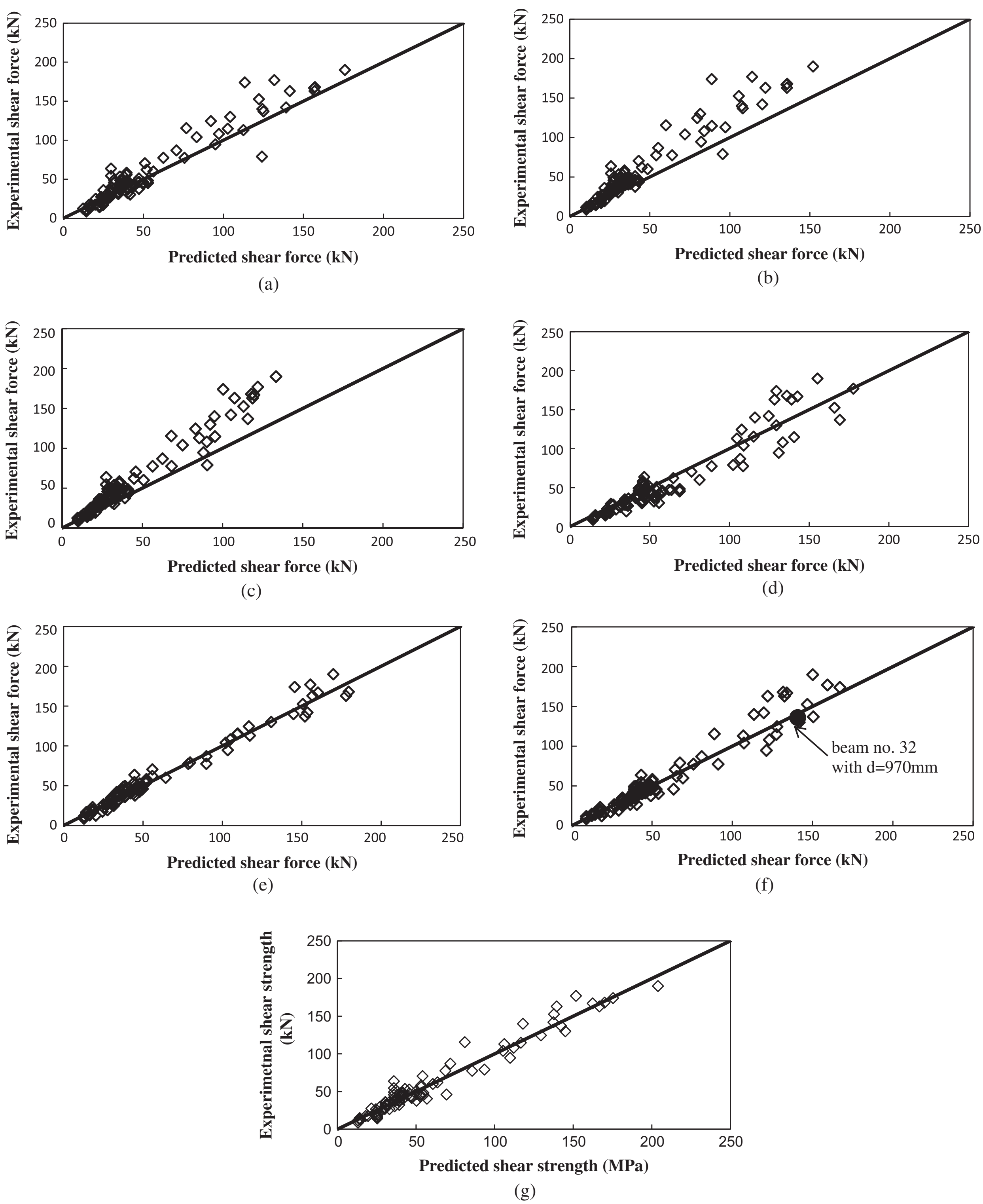

Fig. 2. Comparisons on V_{cf} between test results and predictions. (a) BISE [17] (Eq. (3)) (b) JSCE [20] (Eq. (6)) (c) El-Sayed et al. [2,14] (Eq. (10)) (d) Razaqpur and Isgor [8] (Eq. (11)) (e) The *AV*641.41 model (f) The developed formula (Eq. (19)) (g) The simplified formula (Eq. (20)).

In Table 1, statistical values for 29 testing data were also presented in parentheses. It can be shown that the developed ANN models predict the 29 testing data less accurately when compared with their predictions on 106 data. The models, however, were able to predict the test results better than Eqs. (1)–(3), (4a), (4b), (5a), (5b), (6)–(12).

4.2. Stability of predictions

In Fig. 3, the stability of the four equations (Eqs. (3), (6), (10), and (11)) and the *AV*641.41 model with respect to the change in a/d is presented. A stable prediction for a particular parameter is assumed to be made by the equation or model if the ratios of $V^t_{cf,i}/V^p_{cf,i}$ remain close to 1.0 for the entire range of that particular parameter's values. The solid lines in Fig. 3 represent the best exponential fitting curves for the distribution of $V^t_{cf,i}/V^p_{cf,i}$ values of the 106 data points. As shown in Fig. 3, Eqs. (3), (6), and (10) show a decreasing trend of $V^t_{cf,i}/V^p_{cf,i}$ as a/d increases since they did not include the effect of a/d. As a result, these equations underestimated the V_{cf} for relatively lower a/d values and overestimated the V_{cf} for relatively higher a/d values. Eq. (11) and the *AV*641.41 model, which take into account the effect of a/d in their predictions, showed stability with respect to the change in a/d. Better stability of the *AV*641.41 model compared to Eq. (11) can be seen for a/d by comparing Fig. 3(d) and (e).

In Fig. 4, the stability of Eqs. (3), (6), (10), and (11) as well as the *AV*641.41 model was compared for the remaining parameters of $E_f \cdot \rho_f$, d, b_w, and f'_c. For clarity in presentation, only the best-fitting curves are compared in Fig. 4. Although all predictions included the effect of axial rigidity of $E_f \cdot \rho_f$, Fig. 4(a) shows that the developed *AV*641.41 model maintained better stability than the other predictions. Similar trends were shown in Fig. 4(b), (c) and (d) in that the developed *AV*641.41 model remained more stable than other predictions for the parameters of d, b_w, and f'_c .

5. Parametric studies

Using the developed model, parametric studies were performed to investigate the effects of f'_c, $E_f \cdot \rho_f$, a/d, b_w and d on V_{cf}. For the purpose of the parametric studies, a standard rectangular section was determined. Its dimensions, material properties and reinforcement were selected by taking the approximate average values within the range of the given 106 data. The standard section was selected with b_w = 250 mm, d = 250 mm, a/d = 4.0, E_f = 1.0 × 10^5

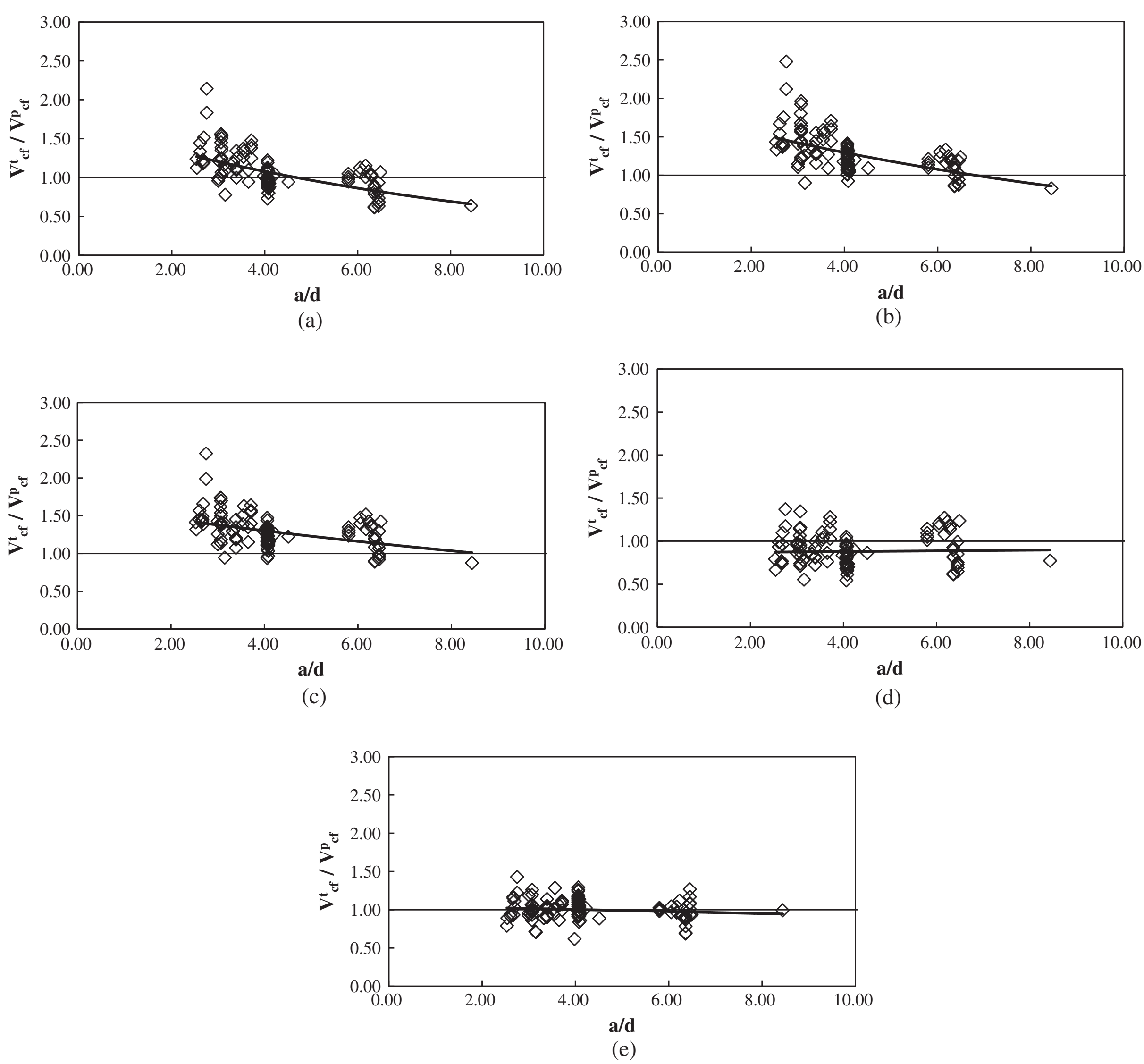

Fig. 3. Stability of different predictions for shear span-to-depth ratio. (a) BISE [17] (Eq. (3)) (b) JSCE [20] (Eq. (6)) (c) El-Sayed et al. [2,14] (Eq. (10)) (d) Razaqpur and Isgor [8] (Eq. (11)) (e) The *AV*641.41 model.

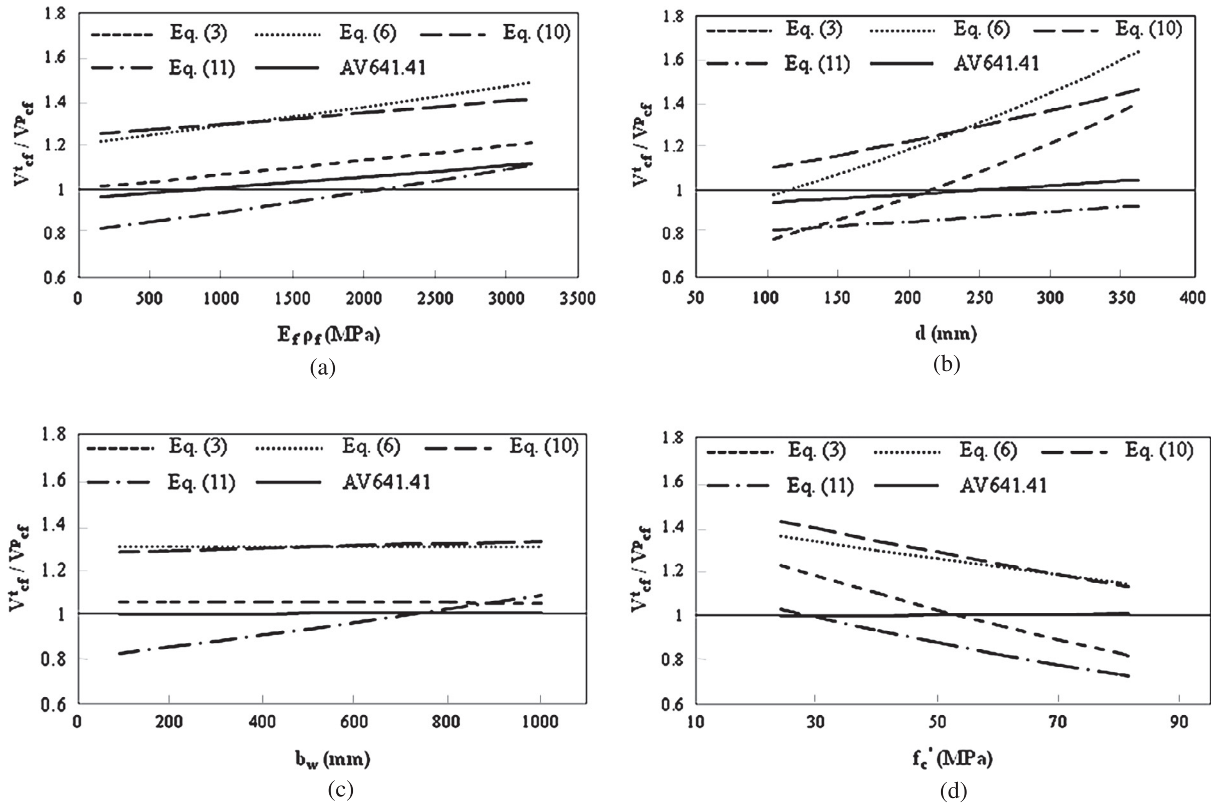

Fig. 4. Stability of different predictions for each parameter. (a) Axial rigidity of FRP bars, (b) effective depth, (c) web width, (d) compressive concrete strength.

MPa and $\rho_f = 0.01$ with $E_f \cdot \rho_f = 1.0 \times 10^3$ MPa and $f_c' = 40$ MPa. Different values for each parameter were input into the *AV*641.41 model and their effects on the shear strength were examined. Predictions from Eqs. (3), (6), (10), and (11) were also made and compared with those by the *AV*641.41 model as shown in Fig. 5.

Fig. 5(a) shows that the shear strength increases with increasing concrete strengths from $f_c' = 25$ MPa to 70 MPa. As Eq. (11) considered the contribution of f_c' to V_{cf} with $(f_c')^{1/2}$, a more rapid increase in V_{cf} was observed with an increase in f_c' than Eqs. (3) and (6) with $(f_c')^{1/3}$ and Eq. (10) with $(f_c')^{1/6}$. The *AV*641.41 model, however, exhibited the least influence of f_c' on the increase in V_{cf}. This might reflect the lesser contribution of concrete to V_{cf} both from the uncracked portion in compression zone and the cracked portion due to the wide shear cracks at the ultimate state resulting from axially less stiff FRP flexural reinforcements. More test results are, however, needed to verify the effect of f_c' on V_{cf}.

Fig. 5(b) illustrates the effects of the axial rigidity of FRP bars. It is worth noting that the same contribution of axial rigidity of FRP reinforcement of $(E_f \cdot \rho_f)^{1/3}$ was given by Eqs. (3), (6), (10), and (11). This is reflected in Fig. 5(b), in which V_{cf} increased in proportion to the increase in $(E_f \cdot \rho_f)^{1/3}$. The *AV*641.41 model also showed similar proportionality of V_{cf} on $(E_f \rho_f)^{1/3}$.

Fig. 5(c) shows the influence of a/d on V_{cf}. Since Eqs. (3), (6), and (10) did not consider the effect of a/d on V_{cf}, their predictions on V_{cf} made by these equations remained the same for different a/d values. Both Eq. (11) and the *AV*641.41 model predicted inversely proportional relations between a/d and V_{cf}. In Eq. (11), V_{cf} is influenced by $k_m = (V_F d/M_F)^{2/3}$, which represents the interactive effect of shear and moment at a section of a slender beam with $a/d \geqslant 2.5$ [11–13].

For four- or three-point loading conditions, k_m in Eq. (11) may represent $(a/d)^{-2/3}$. According to Fig. 5(c), the ratio of V_{cf} at $a/d = 6.0$ to V_{cf} at $a/d = 3.0$ was 49.4 kN/78.4 kN = 0.63 by Eq. (11), which corresponds to the $(6.0/3.0)^{-2/3} = 0.63$. It is interesting to observe that the *AV*641.41 model predicted the ratio of V_{cf} at $a/d = 6.0$ to V_{cf} at $a/d = 3.0$ as 41.5 kN/52.4 kN = 0.79, which approximately corresponds to $(a/d)^{-1/3} = (6.0/3.0)^{-1/3} = 0.79$. As can be seen in Fig. 3(d) and (e), on average, Eq. (11) overestimated V_{cf} compared to the *AV*641.41 model for the entire range of a/d values. The smaller exponent of 1/3 in absolute value that was estimated from the predictions of *AV*641.41 model may partially explain this. Fig. 3(d) shows that Eq. (11) may result in better predictions if they were reduced by 0.12 on average, which is close to $0.79 - 0.63 = 0.16$.

Linearly proportional relationships between b_w and V_{cf} are plotted in Fig. 5(d), which agrees with the generally accepted shear failure mechanism. In Fig. 5(e), the effects of d on V_{cf} are plotted for the different equations and the *AV*641.41 model. As Eqs. (3) and (6) predict V_{cf} in proportion to $d^{3/4}$ and Eqs. (10) and (11) predict it in proportion to $d^{1.0}$, an almost linear increase in V_{cf} with an increase in d was observed. The V_{cf} predicted by the *AV*641.41 model also followed this trend with a slightly more rapid increase with the increase in d.

The parametric studies indicated that the classification of the given data by the trained ANN model could reliably produce the V_{cf}s within the range of test data. Comparisons with other predictive equations, however, revealed some inconsistencies with respect to the effects of f_c' and a/d. The authors believe that this finding resulted from the insufficient amount of experimental data generated for the effects of these parameters or from the adaptation of these effects that were developed for the reinforced concrete beam with steel reinforcement. Therefore, further experimental investigations are needed to verify the effects of f_c' and a/d on V_{cf}.

6. Formulation of predictive equation for shear strength

The application of the developed ANN model to a practical design might be hindered unless the source file of the trained ANN

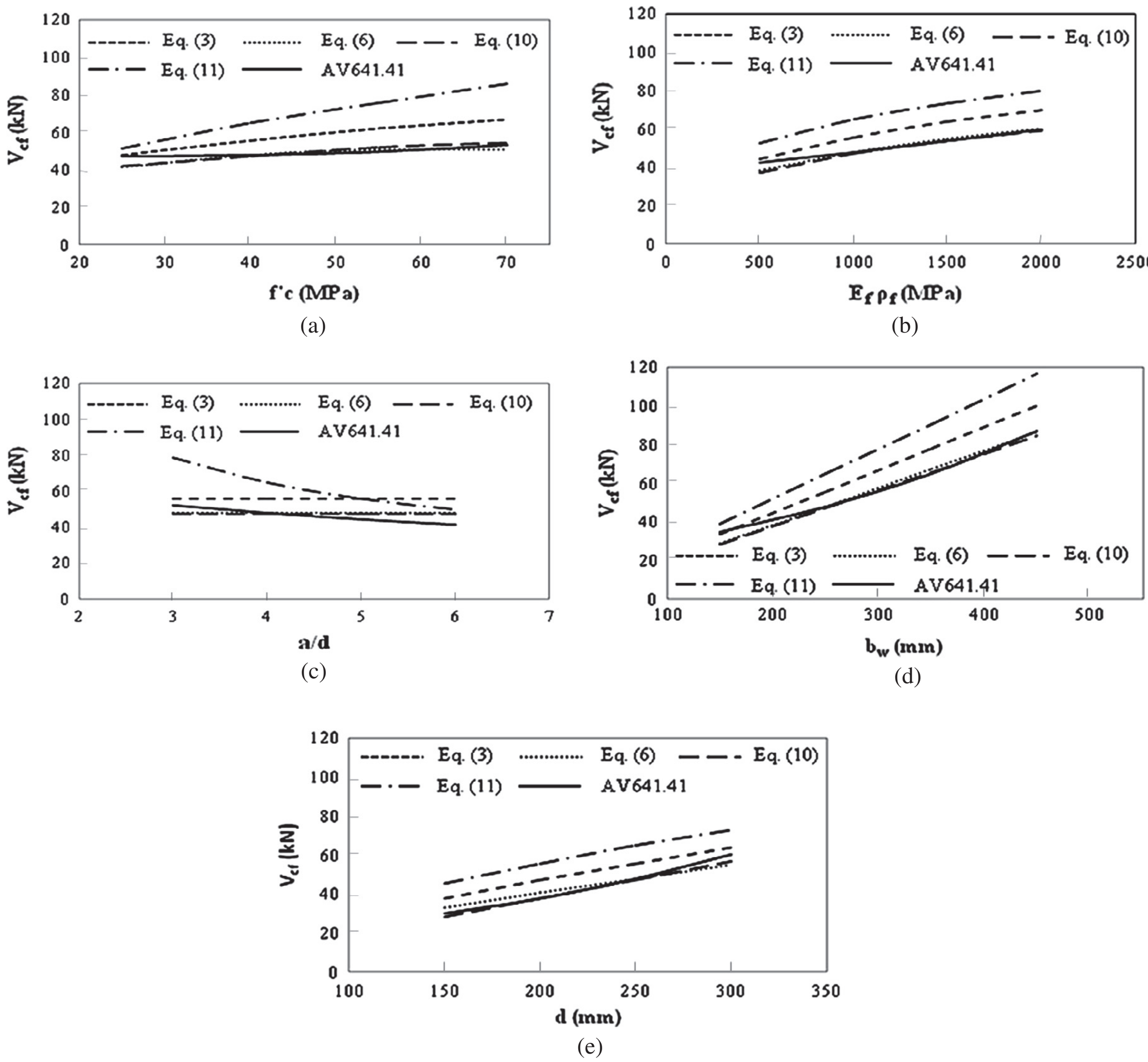

Fig. 5. Effect of each parameter on V_{cf}. (a) Compressive concrete strength, (b) axial rigidity of FRP bars, (c) shear span-to-depth-ratio, (d) web width, (e) effective depth.

model is available at hand. Since new data on V_{cf} can be generated by the developed ANN model for the given set of arbitrary input parameters in the range of training, these data can in turn be used to formulate the predictive equations.

As a preliminary step in formula development, the influence of each parameter on V_{cf} was investigated with 2^k factorial experiment. For the practicality and simplicity of the formula, the AV_b441.41 model is preferred to the AV641.41 model since the AV_b441.41 model requires only four input parameters (f_c', $E_f \rho_f$, a/d and d). Although the AV_b441.41 model requires four input parameters, the AV_b441.41 model showed almost equivalent accuracy as the AV641.41 model (Table 2). The AV_b441.41 model also reflects the direct effect of controlling parameters such as $E_f \cdot \rho_f$ on V_{cf} and the proportionality between b_w and V_{cf}.

6.1. 2^k factorial experiment

The 2^k factorial experiment investigates the effect of k parameters on a shear strength, each at two levels [44]. The complete factorial experiment requires that each level of every parameter occurs with each level of every other parameter, giving a total of 2^k treatment combinations. The individual sums of squares were computed for the effects of the four parameters (f_c', $E_f \cdot \rho_f$, a/d and d) and an additional 12 combinatorial interactive effects on V_{cf}. High and low levels for each parameter were given with reference to those assigned to the standard section within the range of the given data: d = 150 mm and 300 mm; a/d = 3.0 and 6.0; $E_f \cdot \rho_f$ = 1.0 × 10^3 MPa and 2.0 × 10^3 MPa; ρ_f = 0.01 and 0.02; and $f_c' = 40$ MPa and 80 MPa. The results of 2^k factorial experiment indicated that d influences V_{cf} most with the largest percentage of sum of squares of 60.6%, followed by $E_f \cdot \rho_f$ of 19.9%, a/d of 8.1% and f_c' of 5.7% in order. Their interactive effects were shown to be much less significant.

6.2. Formulation

In formulating the predictive formula for V_{cf}, priority was given to the parameters that had a higher influence according to the 2^k factorial experiment. Given the standard section, the AV_b441.41 model was employed to generate shear strengths per unit width (V_{cf}/b_w) for different combinations of four input parameters (d, $E_f \cdot \rho_f$, a/d and f_c'). According to these data, a step-by-step regression analysis was performed to derive the formula.

Fig. 6(a) shows that the increase in V_{cf}/b_w is nearly proportional to the increase in d for different values of $E_f \cdot \rho_f$ and fixed values of a/d = 4.0 and $f_c' = 40MPa$. Fig. 6(b) shows that both the slope (A_1)

and the point of intersection (A_2) for V_{cf}/b_w have an approximately linear relationship with respect to $E_f \cdot \rho_f$ for each fixed a/d value. These relationships can be expressed as:

$$\frac{V_{cf}}{b_w} = A_1 \cdot d + A_2 \tag{15}$$

In Eq. (15), A_1 and A_2 are the linear functions of $E_f \cdot \rho_f$:

$$A_i = B_{i1} \cdot (E_f \cdot \rho_f) + B_{i2} \quad \text{for } i = 1 \text{ and } 2 \tag{16}$$

Fig. 7 illustrates that the four coefficients B_{ij} (i, j = 1 and 2) in Eq. (16) can be approximately represented by the best-fitting straight lines as functions of a/d for a fixed value of f_c':

$$B_{ij} = C_{ij1} \cdot (a/d) + C_{ij2} \quad \text{for } i \text{ and } j = 1 \text{ and } 2 \tag{17}$$

In a similar fashion, the coefficients C_{ij1} and C_{ij2} in Eq. (17) can be represented by the best-fitting straight lines for different f_c' s:

$$C_{ijp} = D_{ijp1} \cdot (f_c') + D_{ijp2} \tag{18}$$

where i, j and p = 1 and 2, and D_{ijpq} with q = 1 and 2 are D_{1111} through D_{2222}. The complete form of Eq. (15) can be given as follows:

$$V_{cf} = k_s' \times b_w \times (g^T \cdot [C] \cdot m) \tag{19}$$

where

g^T = geometry vector = $(a, d, a/d, 1.0)$;

$[C]$ = best-fitting coefficient matrix

$$= \begin{bmatrix} 3.6\times10^{-7} & -1.6\times10^{-5} & -0.5\times10^{-3} & -1.0\times10^{-1} \\ -4.5\times10^{-7} & 4.5\times10^{-4} & 0.7\times10^{-2} & 5.7\times10^{-1} \\ -1.5\times10^{-4} & 7.35\times10^{-3} & -2.7\times10^{-2} & 8.20 \\ 1.56\times10^{-3} & -8.18\times10^{-2} & -1.38 & 6.84\times10^{1} \end{bmatrix};$$

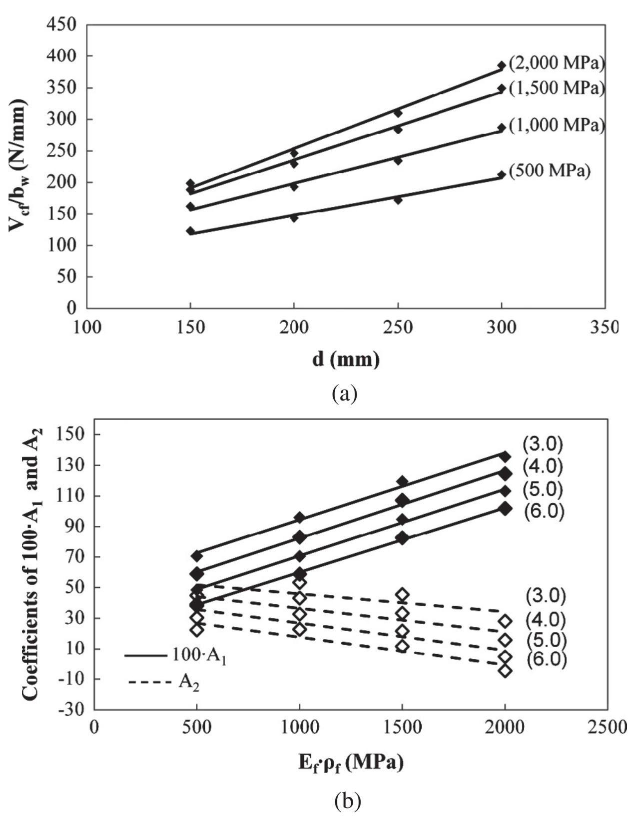

Fig. 6. Linear approximation of V_{cf}/b_w as a function of d and $E_f \cdot \rho_f$ for different a/d and a fixed f_c'. (a) V_{cf} in proportion of effective depth, d for different $E_f \cdot \rho_f$ with fixed $f_c' = 40MPa$ and a/d = 4.0 (b) Coefficients of $100 \cdot A_1$ and A_2 as functions of $E_f \cdot \rho_f$ for different a/d with fixed $f_c' = 40MPa$.

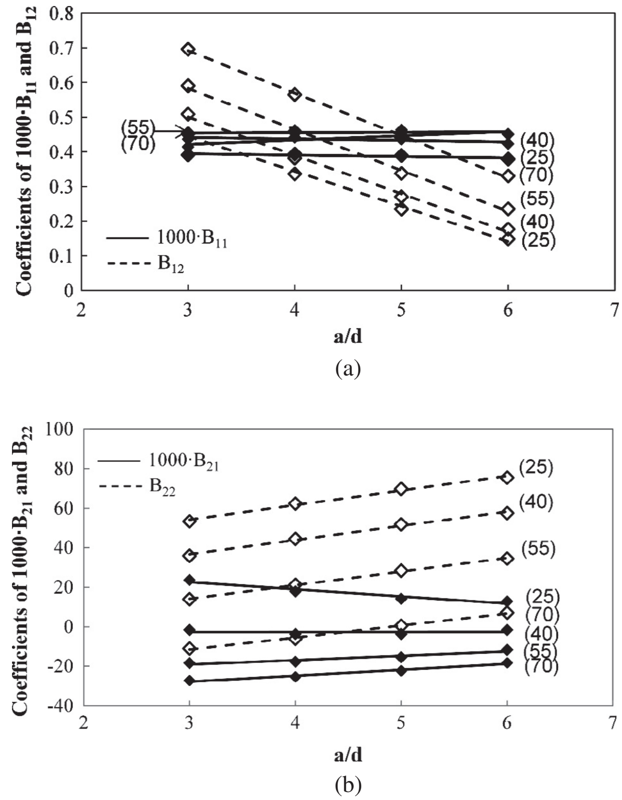

Fig. 7. Linear approximation of coefficients of B_{11}, B_{12}, B_{21} and B_{22} in Eq. (16) as functions of a/d for different f_c'. (a) Coefficients of $1000 \cdot B_{11}$ and B_{12} (b) Coefficients of $1000 \cdot B_{21}$ and B_{22}.

m^T = material vector
$= (E_f \rho_f f_c', E_f \cdot \rho_f, f_c', 1.0)$; and

k_s' = the factor for size effect

$$= \begin{cases} 1.0 & \text{if } d \leqslant 360 \text{ mm} \\ \frac{700}{340+d} & \text{if } d > 360 \text{ mm} \end{cases}$$

The size effect factor k_s in Eq. (11) was adopted and calibrated to derive k_s' in Eq. (19) for continuous transition from the maximum effective depth of d = 360 mm in the data set to larger effective depth of $d \geqslant$ 1000 mm for $k_s' \approx k_s$. Fig. 8 compares the predicted shear strengths by Eq. (19) with those by the AV_b441.41 model and 106 data point test results. The μ, σ, COV, RMSE and R^2 for the ratios of $V_{cf,i}^t/V_{cf,i}^p$ were 1.01, 0.16, 0.16, 0.19 and 0.94, respectively. These statistical parameter values of AV_b441.41 model were shown to be improved compared to the values from Eqs. (1)–(3), (4a), (4b), (5a), (5b), (6)–(11) (Table 1 and Fig. 2). Due to the insufficient amount of data for the beams with an effective depth greater than 300 mm, the developed ANN model could not classify the feature of the size effect feature. When the factor k_s' is used in Eq. (19), V_{cf} = 140.7 kN was obtained for the beam with d = 970 mm (beam no. 32) which was close to the experimentally observed V_{cf} = 136 kN (Fig. 2(f)). Further research, however, is needed to account for the interacting effect of the maximum aggregate size and effective depth of the beam on the shear strength of the FRP-reinforced concrete beam.

For practical applications, a compromise between the accuracy of Eq. (19) and simplicity was made by eliminating the less influence factors:

$$V_{cf} = k_s' \times b_w \times (\Omega_1 \cdot d + \Omega_2 \cdot E_f \rho_f) \tag{20}$$

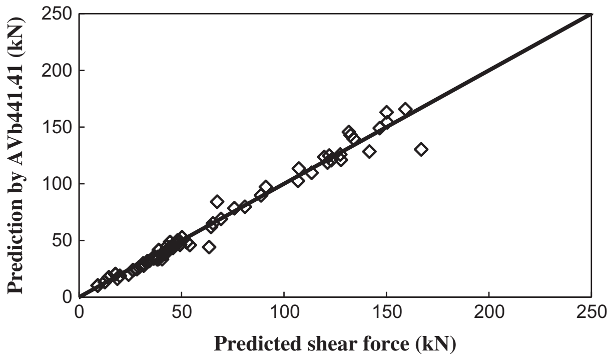

Fig. 8. Comparison between predictions by $AV_b441.41$ and the proposed formula, Eq. (19).

where Ω_1 is the $c_{22} \cdot E_f\rho_f + c_{13} \cdot \frac{a}{d} \cdot f'_c + c_{24}$; Ω_2 is the $c_{41} \cdot f'_c + c_{32} \cdot \frac{a}{d} + c_{42}$; and c_{ij} is the coefficients in the ith row and the jth column in [C] matrix in Eq. (19).

The values of μ, σ, COV, RMSE and R^2 for the ratios of $V^t_{cf,i}/V^p_{cf,i}$ were found to be 1.0, 0.19, 0.19, 0.18 and 0.96, respectively. Although the predictions by Eq. (20) were not as accurate as those by the developed AV641.41 model and Eq. (19), it provides practical estimation of V_{cf} and yet almost equivalent predictions with AV641.41 model and Eq.(19) or even better ones with improved statistical parameter values such as μ, σ and RMSE, compared to those from Eqs. (1)–(3), (4a), (4b), (5a), (5b), (6)–(11) (Table 1 and Fig. 2).

7. Conclusions

Using the existing 106 data point test results, the ANN model and the formulation of predictive equations were developed to predict the shear strength of slender FRP reinforced concrete flexural members without stirrups. The following conclusions were drawn from this study:

1. Previously suggested equations were empirically developed using predefined equations with test data that were mainly generated for a limited number of influential parameters. As a result, most of these equations showed limited accuracy resulting from inconsistent expressions in incorporate the effects of different parameters.
2. For a rational assessment of V_{cf}, research has indicated that six main parameters (f'_c, ρ_f and E_f or $E_f\rho_f$, a/d, b_w and d) need to be incorporated in the model.
3. The dependence of V_{cf} on $E_f \cdot \rho_f$ and the proportionality of V_{cf} to b_w resulted in three different types of inputs (six inputs of f'_c, ρ_f, E_f, a/d, b_w and d; five inputs of f'_c, $E_f\rho_f$, a/d, b_w and d; and four inputs of f'_c, $E_f\rho_f$, a/d and d) and three different types of outputs (V_{cf}, V_{cf}/b_w and V_{cf}/b_wd). For the 288 combinations of different networks resulting from the different numbers of nodes, hidden layers and the different values of the learning rates and momentum parameters, the best ANN models of AV641.41, AV_b441.41 and AV_{bd}541.41 were selected.
4. The AV641.41 model showed superior accuracy to other existing equations and had the most improved statistical parameter values. The values of μ, σ, COV, RMSE and R^2 were 1.01, 0.14, 0.14, 0.16 and 0.98, respectively, for the 106 data points.
5. The AV641.41 model showed stability by maintaining the average of $V^t_{cf,i}/V^p_{cf,i}$ close to 1.0 for the entire range of tested values of the six main parameters. All of the other equations showed worse stability by deviating from 1.0 to some extent.
6. The parametric studies were performed using the standard section. Predictions using the AV641.41 model showed an almost linearly proportional increase in V_{cf} with the increases in $(E_f \cdot \rho_f)^{1/3}$, b_w and d. This trend was similar to that predicted by the other existing equations.
7. The parametric study on the effect of f'_c on V_{cf} exhibited the least influence of f'_c on the increase in V_{cf} compared with those by Eqs. (3), (6), (10), and (11). This might be related to the smaller depth of the compression zone in cracked sections and the wider shear cracks at the ultimate state resulting from axially less stiff FRP flexural reinforcements. More test results are needed to verify the effect of f'_c on V_{cf}.
8. The parametric study showed that the AV641.41 model predicted a less influential effect of a/d than that of Eq. (11). Investigation of the stability of a/d effects showed that, on average, the AV641.41 model better represents the effect of a/d than does Eq. (11).
9. The results of the 2^k factorial experiment indicated that d, $E_f \cdot \rho_f$, a/d and f'_c are influential to the changes in V_{cf} in that order. Their interactive effects were shown to be much less significant.
10. Based on the results of the 2^k experiment and the values of V_{cf}/b_w generated by the AV_b441.41 model, two formulas predicting V_{cf} were developed. The developed formulas provide better predictions than other existing equations, and have improved values of μ, σ, COV, RMSE and R^2.
11. Although the AV641.41 model could not classify the feature of the size effect due to the scarcity of test data with a larger d, the application of the calibrated size effect factor of k'_s to the beam with d = 970 mm resulted in a prediction that was close to its V_{cf}. More data, however, are needed to develop the ANN model to capture the size effect or to justify the use of k'_s.

Acknowledgement

This research was supported by the Chung-Ang University Excellent Student Scholarship in 2013.

References

[1] Joint ACI-ASCE Committee 445. Recent approaches to shear design of structural concrete. J Struct Eng, ASCE 1998;24(12):1375–417.
[2] El-Sayed AK, El-Salakawy EF, Benmokrane B. Shear strength of FRP-reinforced concrete beams without transverse reinforcement. ACI Struct J 2006;103(2):235–43.
[3] Whitehead PA, Ibell TJ. Rational approach to shear design in fiber-reinforced polymer-prestressed concrete structures. J Compos Constr 2005;9(11):90–100.
[4] Yost JR, Gross SP, Dinehart DW. Associate members, ASCE. Shear strength of normal strength concrete beams reinforced with deformed GFRP bars. J Compos Constr 2001;5(4):268–75.
[5] El-Salakawy E, Benmokrane B. Serviceability of concrete bridge deck slabs reinforced with fiber-reinforced polymer composite bars. ACI Struct J 2004;101(5):727–36.
[6] Deitz DH, Harik IE, Gesund H. One-way slabs reinforced with glass fiber reinforced polymer reinforcing bars, fiber reinforced polymer reinforcemnet for reinforced concrete structures. In: Dolan CW, et al., editors., Proceedings of the 4-th international conference, SP-188. Farmington Hills, Mich: American Concrete Institute; 1999. p. 279–86.
[7] Michaluk R, Rizkalla S, Tadros G, Benmokrane B. Flexural behavior of one-way concrete slabs reinforced by fiber reinforced plastic reinforcement. ACI Struct J 1998;95(3):353–65.
[8] Razaqpur AG, Isgor OB. Proposed shear design method for FRP-reinforced concrete members without stirrups. ACI Struct J 2006;103(1):93–102.
[9] Tureyen AK, Frosch RJ. Shear tests of FRP-reinforced concrete beams without stirrups. ACI Struct J 2002;99(4):427–34.
[10] Matta F, Nanni A, Hernandez TM, Benmokrane B. Scaling of strength of FRP reinforced concrete beams without shear reinforcement. In: Fourth international conference on FRP composites in civil engineering; 2008.
[11] Zutty TC. Beam shear strength prediction by analysis of existing data. ACI J, Proc 1968;65(11):943–51.

[12] Khunitia M, Stojadinovic B. Shear strength of reinforced concrete beams without transverse reinforcements. ACI Struct J 2001;98(5):648–56.
[13] ACI Committee 318, Building Code Requirements for Structural Concrete (ACI318-11) and Commentary-ACI318R-02, American Concrete Institute, Farmington Hills, Mich.; 2011.
[14] El-Sayed AK, El-Salakawy EF, Benmokrane B. Shear capacity of high-strength concrete beams reinforced with FRP bars. ACI Struct J 2006;103(3):383–9.
[15] ACI Committee 440, Guide for the Design and Construction of Concrete Reinforced with FRP Bars (440.1R-03), American Concrete Institute, Farmington Hills, Mich., 2003, 41pp.
[16] American Concrete Institute (ACI). Guide for the design and construction of structural concrete reinforced with FRP bars. ACI 440.1R-06, Farmington Hills, Mich; 2006.
[17] British Institution of Structural Engineers (BISE). Interim guidance on the design of reinforced concrete structures using fiber composite reinforcement. IStructE, SETO Ltd., London; 1999.
[18] Canadian Standards Association. Design and Construction of Building Components with Fibre Reinforced Polymers, CSA S806-02, Rexdale, Ontario, Canada; 2002. 177pp.
[19] ISIS Canada. Reinforcing concrete structures with fiber reinforced polymers. ISIS-M03-07, Canadian Network of Centers of Excellence on Intelligent Sensing for Innovative Structures, Univ. of Winnipeg, Winnipeg, Man; 2007.
[20] Japan Society of Civil Engineers (JSCE). Recommendations for design and construction of concrete structures using continuous fibre reinforced materials. In: Machida A, editor. Research committee on continuous fibre reinforced materials, Tokyo, Japan; 1997. 325pp.
[21] Tureyen A, Frosch RJ. Concrete shear strength: another perspective. ACI Struct J 2003;100(5):609–15.
[22] El-Sayed AK, Soudki K. Evaluation of shear design equations of concrete beams with FRP reinforcement. J Compos Constr 2011;15(1):9–19.
[23] Gross SP, Yost JR, Dinehart DW, Svensen E, Liu N. Shear strength of normal and high strength concrete beams reinforced with GFRP bars. In: High performance materials in bridges: proceedings of the international conference, Kona, Hawaii; 2003. p. 426–37.
[24] Fausett LV. Fundamentals of neural networks: architectures, algorithms, and applications. Prentice Hall, Inc.; 1994.
[25] Hecht-Nielsen R. Theory of the backpropagation neural network. In: International Joint Conference on Neural Networks, Washington, DC, 1989. p. :593–605.
[26] Flood I, Kartam N, Associate Members, ASCE. Neural networks in civil engineering I: principles and understand. J Comput Civ Eng 1994;8(2):131–48.
[27] Mansour MY, Dicleli M, Lee JY, Zhang J. Predicting the shear strength of reinforced concrete beams using artificial neural networks. Eng Struct 2004;26:781–99.
[28] Oreta AWC. Simulating size effect on shear strength of RC beams without stirrups using neural networks. Eng Struct 2004;26:681–91.
[29] Cladera A, Mari AR. Shear design procedure for reinforced normal and high-strength concrete beams using artificial neural networks. Part I: beams without stirrups. Eng Struct 2004;26:917–26.
[30] Jung S, Kim KS. Knowledge-based prediction of shear strength of concrete beams without shear reinforcement. Eng Struct 2008;30:1515–25.
[31] El-Sayed A, El-Salakawy E, Benmokrane B. Shear strength of one-way concrete slabs reinforced with fiber-reinforced polymer composite bars. J Compos Constr 2005;9(2):147–57.
[32] Ashour AF. Flexural and shear capacities of concrete beams reinforced with GFRP bars. Constr Build Mater 2006;20:1005–15.
[33] Razaqpur AG, Isgor BO, Greenaway S, Selley A. Concrete contribution to the shear resistance of fiber reinforced polymer reinforced concrete members. J Compos Constr 2004;8(5):452–60.
[34] Lubell A, Sherwwod T, Bents E, Collins MP. Safe shear design of large, wide beams. Concr Int 2004;26(1):67–78.
[35] Gross SP, Dinehart DW, Yost JR, Theisz PM. Experimental tests of high-strength concrete beams reinforced with CFRP bars. In: Proceedings of the 4th international conference on advanced composite materials in bridges and structures (ACMBS-4). Calgary, Alberta, Canada; July 20–23, 2004. p. 8.
[36] Tariq M, Newhook JP. Shear testing of FRP reinforced concrete without transverse reinforcement. In: Proceedings of CSCE 2003-annual conference, Moncton, NB, Canada (CD-ROM).
[37] Alkhrdaji T, Wideman M, Belarbi A, Nanni A. Shear strength of RC beams and slabs. In: Figueiras J, Juvandes L, Faria R, editors. Composites in construction. Lisse, The Netherlands: A. A. Balkema Publishers; 2001. p. 409–14.
[38] Mizukawa Y, Sato Y, Ueda T, Kakuta Y. A study on shear fatigue behavior of concrete beams with FRP beams with FRP rods. In: Non-metallic (FRP) reinforcement for concrete structure, V. 2, proceedings of the third international symposium on non-metallic (FRP) reinforcement for concrete structure. Japan Concrete Institute; 1997. p. 309–16.
[39] Duranovic N, Pilakoutas K, Waldron P. Estes on concrete beams reinforced with glass fiber reinforced plastic bars. Non-metallic (FRP) reinforcement for concrete structure, V. 2, proceedings of the third international symposium on non-metallic (FRP) reinforcement for concrete structure. Japan Concrete Institute; 1997. p. 479–86.
[40] Swamy RN, Aburawi M. Structural implications of using GFRP bars as concrete reinforcement. Non-metallic (FRP) reinforcement for concrete structure, V. 2, proceedings of the third international symposium on non-metallic (FRP) reinforcement for concrete structure. Japan Concrete Institute; 1997. p. 503–10.
[41] Zhao W, Maruyama K. Shear behavior of concrete beams reinforced by FRP rods as longitudinal and shear reinforcement. In: Non-Metallic (FRP) reinforcement for concrete structures, proceedings of FRPRCS-2, L. Taerwe de., Ghent; 1995. p. 352–59.
[42] Yang KH, Ashour AF, Song JK. Shear capacity of reinforced concrete beams using neural network. Int J Concr Struct Mater 2007;1(1):66–73.
[43] Hagan MT, Demuth HB, Beale MH. Neural network design. Boston, MA, USA: PWS; 1996.
[44] Walpole RE, Myers RH. Probability and statistics for engineers and scientists. 9th ed. Prentice-Hall; 2011.